Nonlinear focal shift beyond the geometrical focus in moderately focused acoustic beams

Francisco Camarena,[a] Silvia Adrián-Martínez, Noé Jiménez, and Víctor Sánchez-Morcillo
Institut d'Investigació per a la Gestió Integrada de les Zones Costaneres, Universitat Politècnica de València, C/Paranimf 1, 46730 Grau de Gandia, Spain

(Received 6 June 2012; revised 1 November 2012; accepted 26 December 2012)

The phenomenon of the displacement of the position along the axis of the pressure, intensity, and radiation force maxima of focused acoustic beams under increasing driving voltages (nonlinear focal shift) is studied for the case of a moderately focused beam. The theoretical and experimental results show the existence of this shift along the axis when the initial pressure in the transducer increases until the acoustic field reaches the fully developed nonlinear regime of propagation. Experimental data show that at high amplitudes and for moderate focusing, the position of the on-axis pressure maximum and radiation force maximum can surpass the geometrical focal length. On the contrary, the on-axis pressure minimum approaches the transducer under increasing driving voltages, increasing the distance between the positive and negative peak pressure in the beam. These results are in agreement with numerical KZK model predictions and the existed data of other authors and can be explained according to the effect of self-refraction characteristic of the nonlinear regime of propagation.
 [http://dx.doi.org/10.1121/1.4812865]

PACS number(s): 43.25.Cb, 43.25.Jh, 43.25.Qp, 43.25.Zx [PBB] Pages: 1463–1472

I. INTRODUCTION

The study of the acoustic field characteristics generated by focusing sources, both in linear[1–3] and nonlinear[4–8] regimes, is a continuously developing field of research as sound beams are relevant in most of the ultrasonic applications in medicine and industry. Lucas and Muir[3] studied the acoustic field generated by a focused source in linear regime. This work showed that due to the diffraction of the beam, the on-axis pressure maximum position is not located at the geometrical focus but closer to the source. The distance between these two points is called the linear focal shift and depends on the source characteristics (aperture, geometrical focal length, and frequency) and the medium properties.[9]

The nonlinear focal shift phenomenon, defined as the shift of the maximum pressure (and also intensity and radiation force) position along the axis of focused acoustic beams under increasing driving voltages, has also been discussed and interpreted in previous works. In 1980, Bakhvalov *et al.*[10] predicted a shift in the position of the on-axis pressure maximum in unfocused beams where a migration of the location of the maximum was shown, first away from and then toward the transducer, as the exciting voltage of the source was increased. Duck and Starritt[11] (1986) studied this phenomenon in slightly focused sources as those used in commercial medical pulse-echo equipments, showing that the nonlinear focal shift exists for on-axis maximum and minimum pressure, with different behavior. Averkiou and Hamilton[12] (1997) observed this phenomenon experimentally in a moderately focused piston (linear gain $G = p/p_0 = 10.36$; where p is the value of the pressure in the geometrical focus and p_0 the pressure at the surface of the transducer). The nonlinear focal shift phenomenon was reported by Makov *et al.*[13] in low gain transducers and discussed in terms of the harmonics nonlinearly generated during the propagation of a finite amplitude wave. They provided also experimental evidence of the nonlinear shift in slightly focused transducers ($G = 4$). Recently, Bessonova *et al.*[14] reported a numerical study where the nonlinear focal shift is shown for a moderately focused piston ($G = 10$) in a range of intensity covering both the shift of the maximum pressure toward the geometrical focus at first, even passing beyond the focus, and then the shift backward to the transducer. They also provided an interpretation of the phenomenon based on the self-defocusing effect due to the asymmetrical distortion of the wave profile and to the increase in propagation velocity of the compressive phase of the wave close to the beam axis.

The nonlinear focal shift phenomenon depends, as do most of the characteristics of the high power focused ultrasound beams, on the wave amplitude, the medium properties, and the source physical characteristics (frequency, aperture, and geometrical focal length).[14,15] Two of them, the source physical characteristics and the wave velocity in the medium, can be described through a single parameter, the Fresnel number. This parameter, defined as $N_F = a^2/\lambda F$, where a is the transducer radius, λ the wavelength, and F the geometrical focal length, is widely used in optics and allows classifying the sound beams according to low ($N_F \sim 1$) or high ($N_F > 1$) focusing degree. As discussed in Ref. 13, the Fresnel number is proportional to the linear gain ($G = \pi N_F$); however, because, due to the linear focal shift phenomenon, the real gain ($G_r = p_{max}/p_0$ where p_{max} is the on-axis pressure maximum and p_0 the pressure in the surface of the transducer) is different from G (linear gain), we adopt N_F to

[a]Author to whom correspondence should be addressed. Electronic mail: fracafe@fis.upv.es

TABLE I. Historical studies where nonlinear focal shift evidences have been reported. Water has been used in all the experiments.

Reference	Source characteristics			Nonlinear focal shift p_+ (mm)	Nonlinear focal shift p_+ (Δ_{NL}) (%)	N_F
	Frequency (MHz)	Radius (mm)	Focus (mm)			
Makov *et al.*, 2006 (Ref. 9)	1	15	117	24	20	1.28
Duck *et al.*, 1986 (Ref. 11)	3.5	6.5	70	15	21	1.4
Duck *et al.*, 1986 (Ref. 11)	2.25	9.8	90	∼17	19	1.51
Duck *et al.*, 1986 (Ref. 11)	5	6.5	80	∼8	10	1.8
Averkiou *et al.*, 1997 (Ref. 12)	2.25	18.8	160	∼11	7	3.34
Canney *et al.*, 2008 (Ref. 8)	2	21	44.4	<1	<2	13.37

characterize the focusing of the sound beam in this work. Note that G only estimates the magnification of the beam in the absence of focal shift.

Table I shows the characteristics of the ultrasonic sources (and the corresponding Fresnel number) used in previous studies related with the nonlinear focal shift phenomenon. The table is arranged in increasing Fresnel number (last column) and demonstrates the inverse relation between the Fresnel number and the magnitude of the maximum pressure nonlinear focal shift normalized to the geometrical focal length (Δ_{NL}; penultimate column) as discussed in Ref. 13 from numerical solution of the Khokhlov—Zabolotskaya–Kuznetsov (KZK) equation: The higher the focusing degree the smaller the nonlinear focal shift.

Figure 1 shows the maximum pressure nonlinear focal shift experimental results obtained in the last decades (data from Table I) and the KZK simulations (curve). The curve has been performed by simulating different transducer geometries, from low amplitudes (linear regime, ∼20 kPa in the focus) to sufficiently large amplitudes (∼4–5 MPa in the focus) to reach saturation in the maximum pressure shift, according to the procedure followed in Ref. 13. A global agreement can be observed, even considering that the experiments were not optimized for the observation of the nonlinear focal shift.

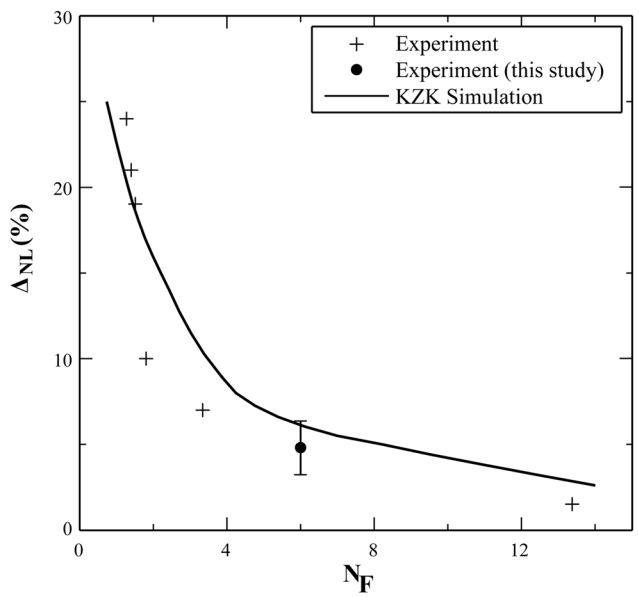

FIG. 1. Nonlinear focal shift in the maximum pressure evaluated in different experiments from 1986 to actual date. The dot represents the result obtained in the present study.

Although the nonlinear focal shift phenomenon has been observed and discussed in previous studies[8–14] for slightly focused beams, a specific study with the objective to analyze, experimentally and numerically, the focal region of moderate Fresnel number transducers ($4 < N_F < 8$) and the magnitude of this shift is absent, as can be seen in Fig. 1. This is a focusing region of special interest because self-refraction plays a more important role than in highly focused beams (like HIFU devices, where the volume of the focus is too small to produce significant self-refraction effects) and in weakly focused beams (where high voltages have to be applied to the transducer to reach the amplitudes necessary to observe nonlinear effects). Also, numerical simulations[13,14] of moderate Fresnel number transducers predict that the on-axis pressure maximum position could surpass the geometrical focal point due to the effect of nonlinearity. We present the first experimental demonstration and explanation of this phenomenon in the current study.

Additionally, a detailed analysis of the acoustic field of moderately focused beams, the location of the significant points like maximum pressure, minimum pressure, maximum intensity, or maximum radiation force as well as the nonlinear focal shifts may become relevant in those applications where moderately focused ultrasound is used, as for example in the transcranial ultrasonic propagation for the blood brain barrier (BBB) opening,[16] where typical focusing transducers are $N_F \sim 6$, or in thermal applications, which aim to widen the focal area to reduce the treatment times[17] ($N_F \sim 10$).

Therefore the aim of this work is to evaluate the nonlinear focal shift of an ultrasonic beam with moderate Fresnel number ($N_F = 6$, with a corresponding linear gain $G = 18.8$) in pressure, intensity, and radiation force as well as to demonstrate that the nonlinear focal shift effect is able to move the real focus beyond the geometrical focus. The pressure waveforms of the ultrasonic beam have been measured under linear and nonlinear conditions and the spatial distributions of peak pressures, intensity, and radiation force have been calculated. Numerical solutions based on the KZK equation and known analytical solutions have been compared with experimental data. The knowledge of the dynamic behavior of the on-axis pressure, intensity, and radiation force distributions provided in this work could be relevant to better characterize the effects produced by ultrasonic focused beams in different medical applications as: HIFU (maximum heat

deposition), cavitation (negative pressure) or imaging[18–21] (radiation force).

II. MATERIALS AND METHODS

A. Experimental set-up

The experimental setup follows the classical scheme of confronted emitting transducer and receiving calibrated membrane hydrophone in a $0.75\,\text{m} \times 0.6\,\text{m} \times 0.5$ -m water tank filled with degassed and distilled water as shown in Fig. 2. The ultrasound source was formed by a plane single element piezoceramic crystal (PZ 26, Ferroperm Piezoceramics, Denmark) mounted in a custom designed steel housing and a methacrylate focusing lens with diameter 50 mm and radius of curvature $R = 70$ mm. The resonant frequency of the system was 2.227 MHz, the radius $a = 25$ mm, and the geometrical focal length $F = 157$ mm, obtained from the expression

$$F = \frac{R}{1 - c_m/c_l}, \tag{1}$$

where c_m is the sound velocity in the medium (water), c_l the sound velocity in the methacrylate (2711 m/s), and R the lens radius of curvature.[22]

The transducer was driven with pulse bursts (150 cycles-sine wave bursts) using a function generator (14 bits, 100 MS/s, model PXI5412, National Instruments) and a linear RF amplifier (ENI 1040L, 400W, +55dB, ENI, Rochester, NY). To measure the acoustic waveforms, a NTR PVDF membrane hydrophone (0.2229 V/MPa sensitivity, model MH2000B with 200 μm active diameter, NTR/Onda) and a digitizer (64 MS/s, model PXI5620, National Instruments) were used. A three-axis micropositioning system (OWIS GmbH) was used to move the hydrophone in three orthogonal directions with an accuracy of 10 μm. All the signal generation and acquisition process were based on a National Instruments PXI-Technology controller NI8176, which also controls the micropositioning system.

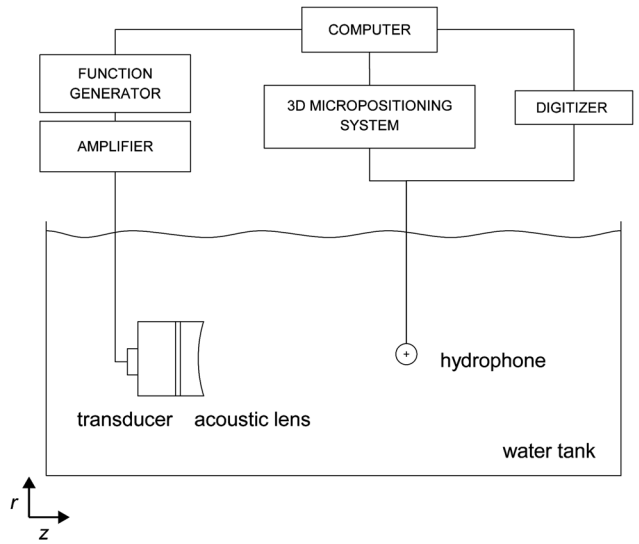

FIG. 2. Scheme of the experimental set up for the pressure measurement in water.

B. Numerical model

Numerical modeling of the experiment was performed using the KZK equation for axi-symmetric beams[23,24]

$$\frac{\partial^2 p}{\partial t' \partial z} = \frac{c_0}{2}\left(\frac{\partial^2 p}{\partial r^2} + \frac{1}{r}\frac{\partial p}{\partial r}\right) + \frac{\delta}{2c_0^3}\frac{\partial^3 p}{\partial t'^3} + \frac{\beta}{2\rho_0 c_0^3}\frac{\partial^2 p^2}{\partial t'^2}, \tag{2}$$

where $t' = t - z/c_0$ is a retarded time, c_0 the sound propagation speed, δ the sound diffusivity, β the coefficient of nonlinearity, and ρ_0 the ambient density of the medium. Equation (2) is valid in the paraxial approximation[25] ($F/a \gg 1$ and $ka \geq (F/a)^{1/3}$) and takes into account nonlinearity, diffraction, and thermoviscous absorption. This equation is solved by means of the numerical scheme described in Ref. 23. Equation (2) can be written in dimensionless variables as

$$\frac{\partial^2 P}{\partial \tau \partial \sigma} = \frac{1}{4G}\Delta_\perp P + A\frac{\partial^2 P}{\partial \tau^2} + NP\frac{\partial P}{\partial \tau}, \tag{3}$$

where $\tau = \omega_0 t'$ is the dimensionless time, $\sigma = z/F$ is the dimensionless axial coordinate, $\rho = r/a$ is the dimensionless radial coordinate, $P = p/p_0$ is the normalized pressure, $\Delta_\perp$ is the transversal Laplacian operator, $G = z_d/F$ is the diffraction parameter or the gain, $A = F/z_a$ is the absorption parameter, and $N = F/z_s$ is the parameter of nonlinearity. Here, $z_d = ka^2/2$ is the characteristic diffraction length (Rayleigh distance), $z_a = 2c_0^3/\delta\omega_0^2$ is the characteristic absorption length and $z_s = c_0^3\rho_0/\beta p_0\omega_0$ is the plane wave shock formation distance.

Simulations were performed in water for beams of initially harmonic pulse burst waves with uniform pressure amplitude at the source. The acoustic source used in the present experiment meets the paraxial condition ($F/2\,a = 3.1$), so the source condition for a moderately focused piston ($G = 18.7$) can be modeled by means of delaying the time waveforms over the plane $z = 0$, as[23]

$$P(\sigma = 0, \rho, \tau) = F(\rho, \tau + G\rho^2), \tag{4}$$

where the source function $F(\rho, \tau)$ is defined as

$$F(\rho, \tau) = f(\tau)H(1 - \rho), \tag{5}$$

where $H(\rho)$ is the Heaviside step function defined in this case by $H(1-\rho) = 1$ for $\rho \leq 1$ and $H(1-\rho) = 0$ for $\rho > 1$, and $f(\tau)$ is the time delayed waveform (sinusoidal pulse burst). Thus simulation parameters were $c_0 = 1486$ m/s, $\rho_0 = 998\,\text{kg/m}^3$, $\beta = 3.5$, $\delta = 5.13 \cdot 10^{-6}$ m^2/s, $F = 157$ mm, $a = 25$ mm, and 25 different values of p_0 ranging from 2 to 99 kPa. These physical parameters leads the dimensionless parameters of $G = 18.7$, $A = 0.024$, and 25 equally distributed values of N ranging from 0.0047 to 0.2324. The algorithm described in Ref. 23 employs an operator splitting approach for solving the equation for an incremental step from σ to $\sigma + \Delta\sigma$. The numerical grid parameters were chosen small enough to ensure the solution does not vary less

than 1% at halving the grid refinement. Thus the time step chosen was $\Delta\tau = 0.010$ and leads to 200 samples per cycle; the transversal grid step was $\Delta\rho = 10^{-3}$ and the axial grid step was $\Delta\sigma_{IB} = 10^{-4}$ for the fully implicit backward difference method, and $\Delta\sigma_{CN} = 2 \cdot 10^{-4}$ for the Crank–Nicolson method. First method was applied to solve the field near the transducer ($\sigma < 100\ \Delta\sigma_{IB}$) and beyond this distance Crank–Nicolson method is applied.

C. Measurement procedure

To characterize the nonlinear focal shift phenomenon in the ultrasonic beam emitted by the source, it is necessary to measure the acoustic field on the radiator axis at different initial pressures. Eight increasing and voltage inputs were applied at the transducer terminals: 2 V_{pp} (linear regime), 9, 21, 45, 65, 85, 100, and 125 V_{pp}, to study the evolution of the acoustic field characteristics from linear to nonlinear regime. The voltage values were selected to cover the range homogeneously. As the beamwidth can be quite small (3 mm at the focus in the linear case, −6 dB), a precise positioning of the hydrophone on the radiator axis is required. The axis of the radiator was oriented approximately along the z axis of the micropositioning system. Then the pressure waveforms $p(t,x,y,z)$ were measured in 25 planes along the z axis of the micropositioning system: From 131.3 to 146.3 mm spaced each 3 mm; from 146.3 to 161.3 mm spaced each 1 mm; and from 161.3 to 176.3 mm spaced each 3 mm (see Fig. 3). These planes were transversal to the z axis, 6 mm × 6 mm (x-y planes) and waveforms were acquired with 0.5 mm spatial resolution on them (144 measurement points/plane). Five planes around the geometrical focus were acquired with 0.25 mm spatial resolution. At every point of measure, waveform averaging was performed of multiple tone burst to increase the signal-to-noise ratio. After that, the maximum of the waveform signal was selected by adjusting a Gaussian function to the histogram of maxima in the tone burst. The equipressure curves in each plane built with the selected maxima typically had a circular form: This was indicative of good axial symmetry of the radiator. Finally, from the measurement of the pressure maxima distribution in each x-y plane, we were able to obtain the pressure maximum amplitude and its coordinates (x_{max},y_{max}) in each of the 25 transversal planes; this allowed us to define the radiator axis.

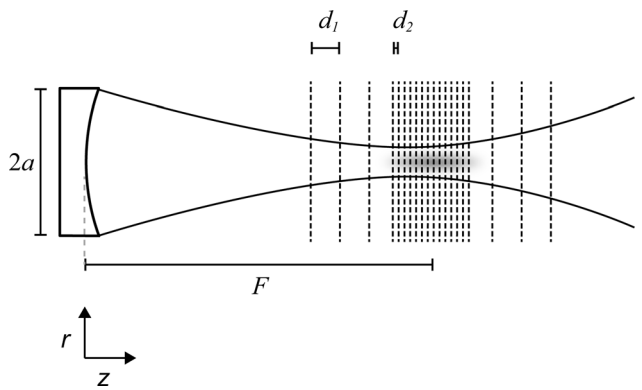

FIG. 3. Measuring procedure. Waveforms are measured in 25 planes along the z axis of the micropositioning system. The slice separation was $d_1 = 3$ mm and $d_2 = 1$ mm.

As the hydrophone displacement along the axis was determined by the micropositioning system with high accuracy (0.01 mm), to locate the hydrophone position with respect to the radiator, it was sufficient to measure the distance between the receiver and the transmitter only at one point on the axis. This was done by measuring the time passing between the tone burst front emission and reception and using the value of the sound velocity at the temperature of water. The accuracy of this measurement was better than 0.3 mm.

Most of the measured planes were located close to the geometrical focus location with minimal separation of 1 mm between them (see Fig. 3). This spatial resolution in z was especially necessary to evaluate the position of the on-axis pressure maximum with an accuracy better than 3 mm, which is the requirement to be sensible to the nonlinear pressure focal shift phenomenon (estimated in less than 1 cm from numeric simulations, Makov *et al.*[13]). In spite of the fact that we measured the on-axis pressure maximum every 1 mm near the geometrical focus, as the measurement of pressure had a random error estimated from 2% (lower pressure) to 4% (higher pressure) in our experiment, the uncertainty in the determination of the location is higher than 1 mm as shown by the error bars in the different plots.

To evaluate the on-axis intensity $I(z)$ and radiation force $F(z)$ distributions, the temporal profiles $p(t,z)$ have been used in the following expressions.

For the intensity,

$$I(z) = \frac{1}{nT}\int_{t_0}^{t_0+nT} \frac{p^2(t,z)}{\rho c} dt, \tag{6}$$

where T is the period, n is an integer, ρ is the water density, and c is the speed of sound.

And for radiation force[26]

$$F(z) = \frac{b}{c^5\rho^3}\left\langle \left(\frac{\partial p(t,z)}{\partial t}\right)^2 \right\rangle, \tag{7}$$

where b is the dissipation and the angular brackets denote temporal averaging over fast acoustic oscillations.

D. Linear characterization of the beam

The characterization of the beam in linear regime is needed to determine the characteristics of the acoustic source (aperture and geometrical focus) and the position of the on-axis pressure maximum, i.e., the linear focal shift. The linear characterization was performed in three steps: First, nominal values (those provided by the lens manufacturer) were used to evaluate the nominal geometrical focal length according to Eq. (1). Next, the analytic O'Neil solution,[1] valid for linear focused fields, was fitted to the experimental data at the lower voltage excitation value of the transducer (2 V_{pp}). This fit provided a new value for the geometrical focal length and aperture and a value for the pressure in the source, $p_0 = 2$ kPa. Finally, KZK simulations were

performed for various values of the source aperture and radius of curvature to obtain the "best fit" to the experimental data in the linear regime.

The geometrical focal length and the aperture of the transducer were nominally stated by the manufacturer as $F = 157$ mm and $2a = 50$ mm, respectively, resulting in $N_F = 6$ (being 2.227 MHz the working frequency), f-number $= 3.14$, and $G = 18.8$. The fit of the analytic O'Neil solution to the experimental data is shown in Fig. 4(a) and provides an effective aperture of the transducer of 51.6 mm and an effective geometrical focal length of 158.2 mm. Figure 4(b) shows a good behavior of the fit also in the transversal distribution of the pressure. And finally, the KZK simulation provides an effective aperture of the transducer of 50.2 mm and a geometrical focal length of 157 mm. The small differences among all three calculations can be due to the fact that linear KZK and O'Neil solutions are different as they are solutions of different diffraction models (parabolic approximation and Rayleigh integral) and to the fact that our transducer is not a perfect piston: The transducer housing, the surface waves and the effect of the lens borders might limit and distort its vibration.[8]

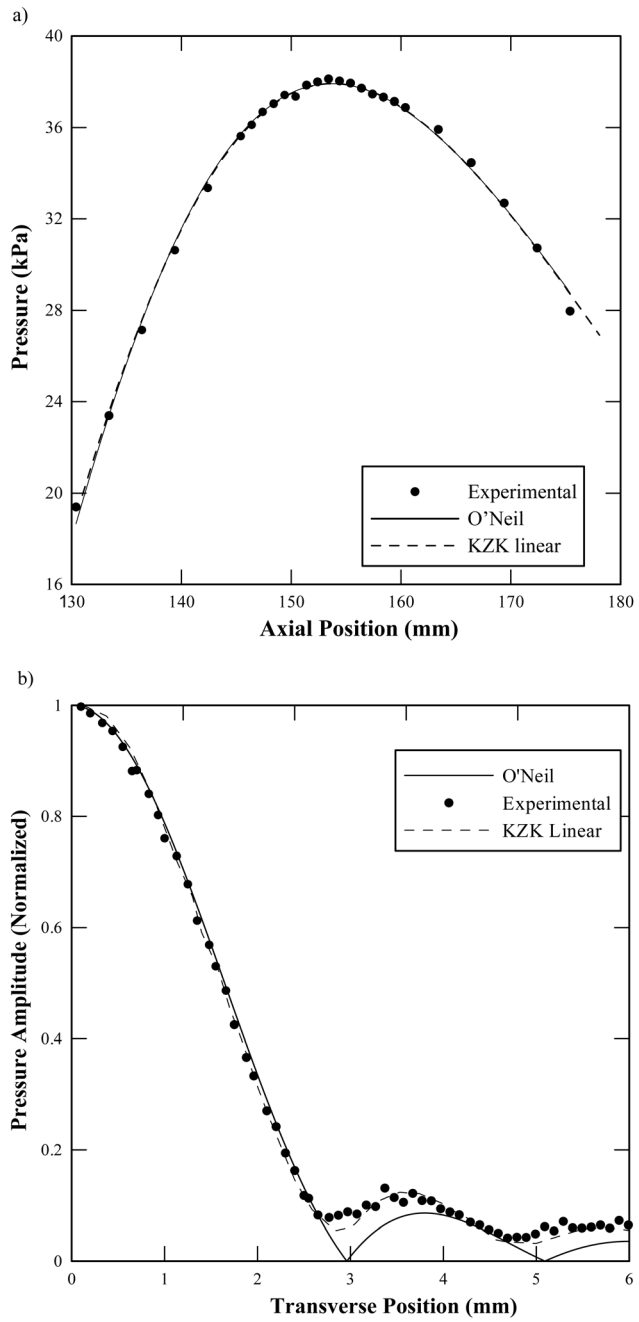

FIG. 4. (a) On axis pressure distribution and (b) transversal normalized pressure in linear regime.

The on-axis pressure maximum obtained in the experiment is located at 154 mm from the transducer, i.e., 97.8% of the geometrical focal length, what is in good agreement with the value of the linear focal shift predicted in Ref. 13 for transducers with Fresnel number 6, i.e., 97%. The results of both models, the O'Neil and the calculated with the "best fit" aperture and geometrical focal length in the KZK simulation, are in good agreement with the experimental data.

Finally, the values of aperture and geometrical focal length obtained by the "best fit" between the experimental values and the KZK simulated values in linear regime will be used to simulate the acoustic field in the nonlinear regime.

III. RESULTS

To study the effect of the nonlinear propagation on the on-axis distribution of the pressure, intensity, and radiation force, acoustic waveforms in front of the emitter were acquired (as described in Sec. II C) for different input voltage applied to the transducer (from 2 to 125 V_{pp}). Figure 5 shows the value and location of the on-axis maximum and minimum pressure measured experimentally (dots). Error bars in the estimation of the maxima locations are due to the errors associated to the measurement of the pressure in our experiment. They range from 1 mm in the linear case (2 V_{pp}) to 3 mm in the higher excitation case (125 V_{pp}), increasing with the voltage input because the transversal area (beam waist) of the focus becomes thinner, and it is increasingly difficult to estimate the value of the maximum pressure in each transversal plane (0.25 mm transversal spatial resolution and 0.2 mm hydrophone active diameter), what implies an increasing of the error in the determination of the axial position of the different maxima. Error bars in the determination of the minima locations are invariant: 1 mm, the minimum distance between the measured planes, as the beamwidth of the negative focus increases with the excitation voltage.

The vertical line in Fig. 5 represents the position of the geometrical focus ($F = 157.4$ mm), estimated as the mean of the three values obtained in Sec. II D with independent methods. The curves represent the on-axis maximum (continuous) and minimum (dashed) pressure values and locations evaluated from the KZK numerical simulation of the experiment. Both experiment and simulation show the same four relevant conclusions: (1) The on-axis pressure maximum position moves away from the transducer when the exciting power increases (until 7.5 mm, corresponding to 4.8% of nonlinear focal shift; see Fig. 1), (2) the on-axis pressure minimum position moves toward the transducer when the exciting

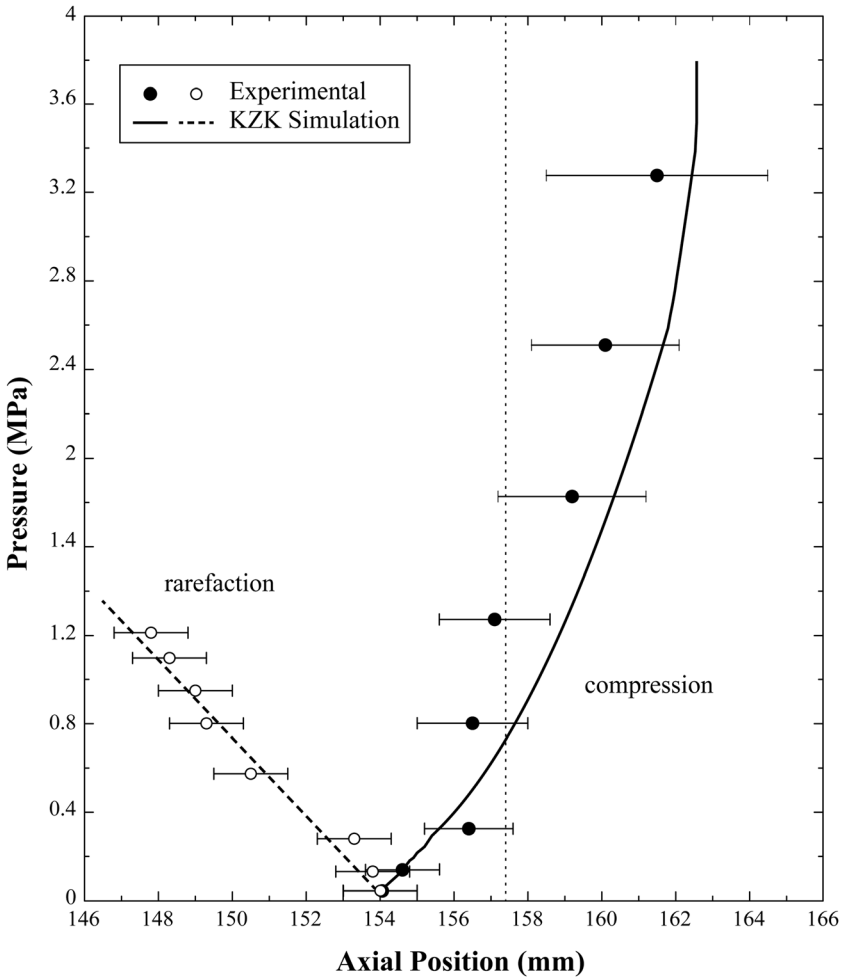

FIG. 5. On axis maximum positive and negative pressures. Experimental values and KZK simulation. Input voltage values are 2, 9, 21, 45, 65, 85, 100, and 125 Vpp from bottom to top.

power increases (6.2 mm), (3) the on-axis pressure maximum can surpass the position of the geometrical focus, and (4) at the highest excitation voltage (125 V_{pp}), the distance between the maximum and the minimum pressure is larger than 1 cm.

The behavior of the maximum and minimum pressure positions presented in Fig. 5 can be understood considering the effect of self-refraction[27] associated to nonlinear propagation. Because the velocity of finite amplitude waves grows with the value of the amplitude, and in a focused beam the amplitude is higher along the propagation axis than in remote regions, the compressive phase of the waves travel faster near the axis. Consequently, a flattening of the wave front is produced, leading to a displacement of the pressure maximum from the source. The contrary effect is produced for the rarefaction phase of the waveform (self-focusing). Due to the asymmetric distortion of the wave profile caused by the combined effects of nonlinearity and diffraction, the propagation velocity of the rarefaction phase decreases on the axis (and the focus)[24] causing an additional focusing of the waveform, and consequently a displacement of the maximum rarefaction pressure toward the source.

Figure 6 shows a simple (ray theory and Snell law) representation of the self-refraction effect for the positive and negative peak pressures. For illustrative purposes, it has been considered that the change in the wave speed is due to a change in the propagation medium (different medium in the paraxial area near the focus), although the effect is due to nonlinear effects. The rays are defocused (b) or focused (c) with respect to the linear case (a) due to the change in the propagation velocity. If the transducer is strongly focused, the focal region becomes too small to produce significant self-refraction effects, which is the reason why HIFU instruments do not suffer large nonlinear focal shift effects.

Experimental and simulated values in Fig. 5 show good agreement in the quasi-linear region (lower input voltages), but they differ slightly as the power increases (nonlinear regime), being the nonlinear focal shift effect higher in the simulation. There are several possible reasons that explain this fact: First, the frequency response of the hydrophone is bounded to 20 MHz, which limits the number of affects harmonics detected by the hydrophone. Second, the sound field does not present a flat and uniform distribution over the active area of the receptor (200 μm active diameter), thus the measure is underestimated after the spatial averaging of the measurement region, on the contrary, the simulation maximum are the KZK solution for an infinitesimal field point. A final source of error is due to the non-uniform vibration of the transmitter as discussed before. These hypotheses have been discussed in detail in Ref. 8. In our case, the finite size of the hydrophone was simulated by averaging over a 200 μm diameter circular cross section, equivalent to active hydrophone diameter. The results show that spatial averaging of the hydrophone sub-predicts the positive peak

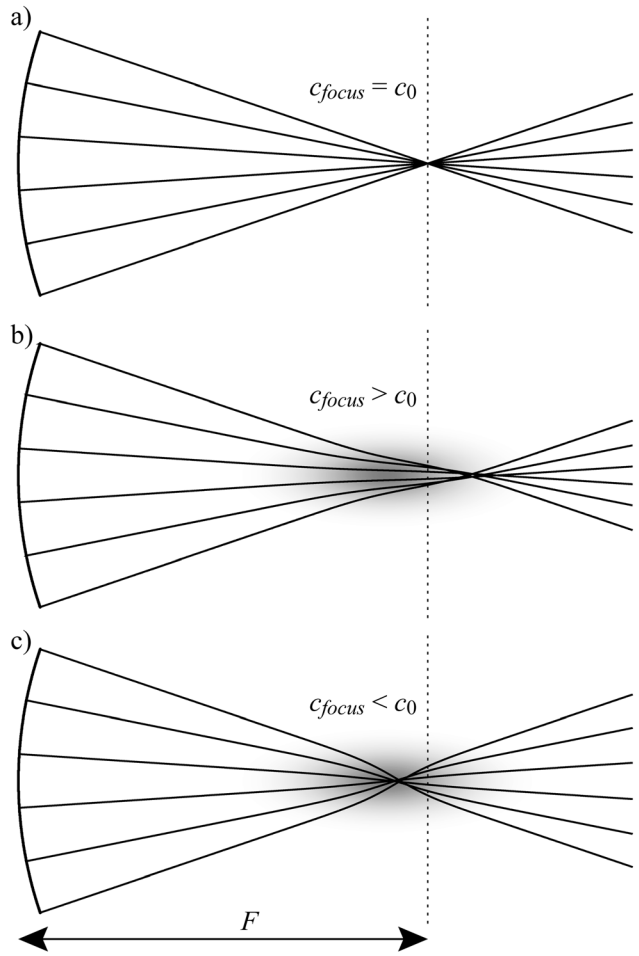

FIG. 6. Geometrical interpretation of the self-refraction phenomenon. Ray theory is considered in the graphs. In (a), the absence of diffraction makes the transducer focus in the geometrical focus in linear regime. In (b), the positive peak are defocused because of the increase of velocity in this phase of the waveform in nonlinear regime, and in (c), the rarefaction phase of the waveform is focused prefocally because the decrease of the velocity.

pressure. The magnitude of the discrepancy linearly varies from 0.6% for low input pressures to 2.1% for 3.7 MPa peak pressures. The finite bandwidth of the hydrophone was simulated by zero-phase filtering the KZK signals by a low pass filter equivalent to the frequency response of the hydrophone. The nonlinear focal shift processed by the filtered signals is sub-predicted and matches the experimental results. These results evidence that the limited bandwidth of the receiver alter the measurement of the beam properties, i.e., the effect of focal displacement will be stronger if all harmonics are recorded. Thus filtering the simulated waveforms with a 20 MHz low pass filter the estimations on the focal displacements varies −1.3% for 3.6 MPa and the peak pressure value varies −6% for 3.6 MPa. Using these uncertainties, the simulated-limited finite size and bandwidth of the hydrophone predictions agrees the experimental measurements, and its order of magnitude is comparable to that measured in other papers.[8]

Figure 5 shows saturation in the on-axis pressure maximum shift. At these intensities, a high amplitude shock develops near the focus [see Fig. 7(d)]. Nonlinear absorption of the wave energy occurs at the shocks and the peak positive pressure decreases, diminishing the self-refraction effect. The saturation effect is not observed in the on-axis rarefaction maximum because the nonlinear absorption affects mainly the higher frequencies (the narrow positive peak).

Previous studies demonstrate that the on-axis pressure maximum shifts toward the source at very high intensities after saturation is reached (numerically[9,14,28] and experimentally[9]). This is due to the presence of shock waves in the prefocal area, where the nonlinear absorption decreases the wave amplitude and consequently reduces the self-defocusing effect.

Figure 8 shows the value and location on the on-axis maximum intensity and radiation force. Intensity, evaluated from Eq. (6), reach a maximum at 120 W/cm^2, which is far

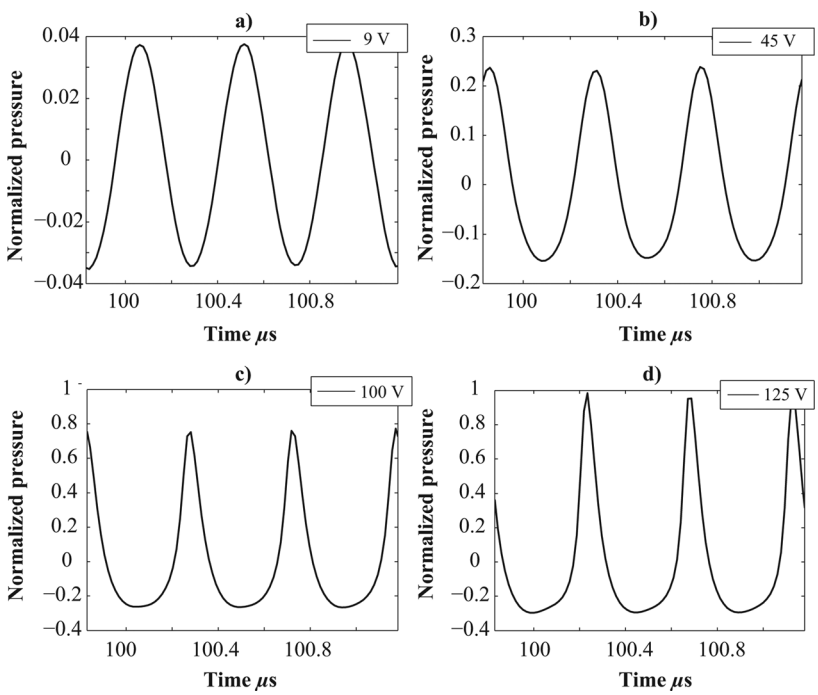

FIG. 7. Time profiles in the geometrical focus at different input voltage.

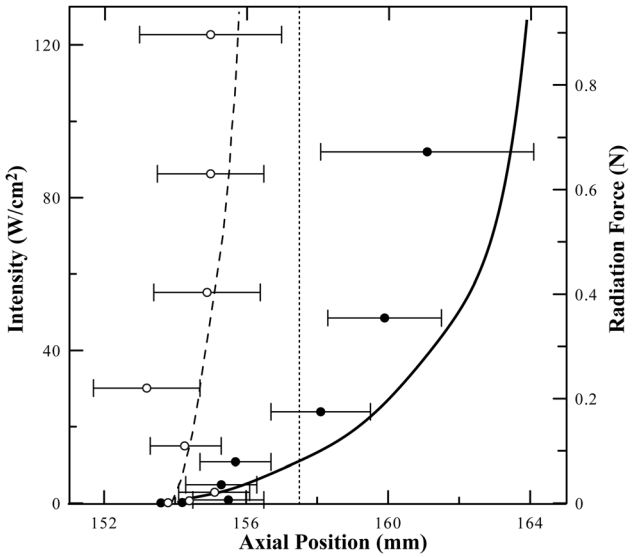

FIG. 8. On-axis maximum intensity and radiation force. Experimental values (dots) and KZK simulation (curves).

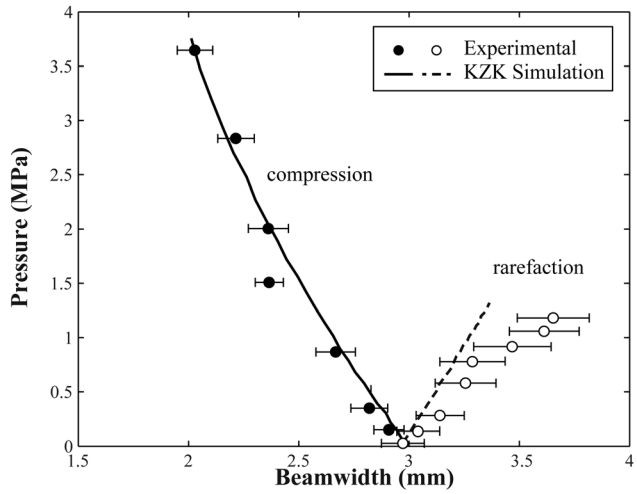

FIG. 9. Compression and rarefaction beamwidth (defined at −6 dB) at the geometrical focus for the different input voltages applied: 2, 9, 21, 45, 65, 85, 100, and 125 V_{pp} from bottom to top. Experimental values (dots) and KZK simulation (lines).

away from the typical values that can be obtained with HIFU devices. A small shift in the location of the on-axis intensity maximum is observed in the KZK simulation (2.3 mm) that agrees with the experimental results, although the error in the estimation of the intensity location is higher than the shift. Previous studies show the same singular behavior for the intensity (Ref. 13): The shift is always smaller than in pressure, and it decreases with the focusing degree of the source. At very high focusing levels (HIFU devices, for example), the shift is insignificant and the on-axis intensity maximum is located at the geometrical focus. However, the radiation force is very sensible to the self-refraction effect. As it can be seen in Fig. 8, the shift is comparable to that observed for the pressure (Fig. 5), both in the experiment and the simulation, even surpassing the geometrical focus. This effect can be important in ultrasound-stimulated vibroacoustography techniques[18–21] (where the radiation force is used to produce displacements in tissue), as the location where the radiation force is applied can change with the amplitude of the excitation wave.

It is important to indicate that the on-axis pressure maximum, pressure minimum, intensity, and radiation force show different behavior under increasing nonlinearity. On-axis maximum and minimum pressure shift behavior has been explained by the self-refraction effect, which can also explain the saturation in the maximum pressure shift due to the nonlinear absorption that appears in the shock waves. As mentioned, the shift in radiation force is very similar to the shift in maximum pressure: Radiation force is proportional to the absorption, which increases with frequency, therefore both will be higher in distorted wave profiles (with more harmonics), which correspond to the more peaked waveforms (higher positive pressure).

However, a different behavior can be observed in the intensity shift, much smaller compared with the maximum pressure shift. The character of the nonlinear deformation of time profiles shown in Fig. 7 provides the clue to understand this discrepancy during the process of nonlinearity development. Actually, the deformation of the time profile lies in the quite fast increase of the profile peak level together with the simultaneous narrowing of this peak, as observed in Fig. 7. This dynamic process is accompanied by a deceleration in the increase of the area under this peak. Under the condition[6]

$$\int_0^T p(t,x,y,z)dt = 0, \tag{8}$$

the comparative growth of the area of the negative part of the profile is also decelerated, and the intensity [as the square of the full area under the curve profile, see Eq. (6)] slows down.[13] This becomes apparent in the lag of nonlinear shift of the intensity maximum compared with the shift of pressure maximum.

As nonlinear effects increase, not only the locations of spatial maxima of pressure, intensity, and radiation force change but also the transversal spatial structure.[24] Figure 9 shows the compression and the rarefaction beamwidth in the geometrical focus at a level of −6 dB in the transverse direction for the different input voltages. In the focal area, compression beamwidth decreases in nonlinear regime (−36%) meanwhile rarefaction beamwidth increases (+36%). This is due to the way nonlinearity distorts the wave in the presence of diffraction. The wave acquires a frequency-dependent phase shift. This leads to the appearance of corresponding phase shifts between the harmonics, which produces an asymmetric profile distortion: Within each period, the compression region becomes higher and sharper and the rarefaction region becomes smoother [see Figs. 7(c) and 7(d)]. The asymmetric profile distortion of the waveform is the responsible of the increase of the real gain (p_+/p_0) in the moderate nonlinear region and the decrease of the negative real gain (p_-/p_0) respect to the linear gain value.[8] So the maximum pressure grows faster in the region near the focus (where the higher distorted waveforms are located) than in the off-axis regions when input excitation in the transducer increases,

reducing the positive beamwidth (and consequently the transversal area of the focus). Contrary, the rarefaction regions of the wave grows more slowly in the propagation axis (and in the focus) than in the regions around the focus because the waveform is more distorted on axis, so the transversal amplitude profile becomes flattened when nonlinearity is higher, increasing the rarefaction beamwidth.

IV. CONCLUSION

The acoustic field of a moderately focused transducer ($N_F = 6$; $G = 18.8$; f-number $= 3.14$) has been studied to determine the characteristics of the linear and nonlinear focal shift in the case of pressure, intensity, and radiation force.

In linear regime, it has been observed that the on-axis pressure maximum is located at 154 mm from the transducer, i.e., before the geometrical focus (157.4 mm), which indicates a linear focal shift of 3.4 mm. This shift agrees with the Makov *et al.*[13] results in their study about the dependence of the linear focal shift with the Fresnel number.

In nonlinear propagation conditions, it has been observed a maximum pressure position displacement (both in experiment and simulation) when the input voltage is increased, even exceeding the geometrical focus. It has also been observed a shift in the on-axis pressure minimum but in the contrary direction (backward). This behavior has been explained by means of the effect of self-refraction, which modifies the focusing conditions with respect to the linear case. When the maximum voltage is applied to the transducer, the on-axis pressure maximum position exceed the geometrical focus in 4 mm, and the separation between the on-axis maximum and minimum positions is as far as 13.7 mm.

The on-axis intensity maximum is located in the linear regime at the same point than the on-axis maximum and minimum pressures (154 mm from the transducer). There is a shift in the position of the maximum intensity when the input voltage to the transducer increases, but it is quite low (2.3 mm) compared to the shift in the pressure (7.5 mm), and it does not surpass the geometrical focus. The reason for the different behavior between them has been explained on the base that the fast growth of the positive peak in a period does no imply an increase in the area subtended by this period (and consequently the intensity).

However, the radiation force follows the same behavior than the maximum pressure because the sharper the positive peak the higher the absorption, increasing the value of the force applied to the medium.

There exists a spatial separation between the points of interest in a beam: Maximum pressure, minimum pressure, intensity, and radiation force, which depend on the Fresnel number and input voltage applied to the transducer. From the results of this work, at the higher input voltage applied, the maximum pressure and the maximum radiation force are located at 161.5 mm from the transducer, the minimum pressure is located at 148 mm and the maximum intensity at 156.3 mm. This dissociation between the relevant points in an ultrasonic beam implies that the effects produced will be also spatially dissociated, what has to be taken into account according to the desired application. In thermal applications of ultrasound,[29] the pressure waveform is important as it determines both, the radiation force and the heat deposition in the medium; rarefaction is responsible of cavitation, so the minimum pressure location will be the region of interest in applications where cavitation takes an important role, as for example in transcranial BBB opening.[16] Finally, radiation force is used in new elastographic techniques as HMI[21] or ARFI[20] to induce displacements of the tissue in the focus of the beam, so that the knowledge of the exact position of the on-axis maximum radiation force applied is crucial.

The nonlinear focal shift studied in this work becomes less important in highly focused beams (as for example, in HIFU devices) because the focal area is smaller and self-refraction effect decreases. However, detailed studies should be conducted if the technique is very sensible to the value and location of the radiation force applied, as it is the case of acoustic radiation force elastography techniques.[30]

ACKNOWLEDGMENTS

We wish to thank Dr. Yuri N. Makov for his advice and remarks for the improvement of this article. This work was supported by Universitat Politècnica de València, under Project Nos. PAID-06-10-002-295 and PAID-05-11-002-340.

[1]H. T. O'Neil, "Theory of focusing radiators," J. Acoust. Soc. Am. **21**, 516–526 (1949).
[2]G. Kossoff, "Analysis of focusing action of spherically curved transducers," Ultrasound Med. Biol. **5**, 359–365 (1979).
[3]B. G. Lucas and T. G. Muir, "The field of a focusing source," J. Acoust. Soc. Am. **72**, 1289–1296 (1982).
[4]E. A. Zabolotskaya and R. V. Khokhlov, "Convergent and divergent sound beams in nonlinear media," Sov. Phys. Acoust. **16**, 39–42 (1970).
[5]V. P. Kuznetsov, "Equation of nonlinear acoustics," Sov. Phys. Acoust. **16**, 467–470 (1970).
[6]N. S. Bakhvalov, Ya. M. Zhileikin, and E. A. Zabolotskaya, *Nonlinear Theory of Sound Beams* (American Institute of Physics, New York, 1987), p. 168.
[7]M. F. Hamilton, V. A. Khokhlova, and O. V. Rudenko, "Analytical method for describing the paraxial region of finite amplitude sound beams," J. Acoust. Soc. Am. **101**, 1298–1308 (1996).
[8]M. S. Canney, M. R. Bailey, L. A. Crum, V. A. Khokhlova, and O. A. Sapozhnikov, "Acoustic characterization of high intensity focused ultrasound fields: A combined measurement and modelling approach," J. Acoust. Soc. Am. **124**, 2406–2420 (2008).
[9]Yu. Makov, V. Espinosa, V. J. Sánchez-Morcillo, J. Cruañes, J. Ramis, and F. Camarena, "Strong on-axis focal shift and its nonlinear variation in low-Fresnel-number ultrasound beams," J. Acoust. Soc. Am. **119**, 3618–3624 (2006).
[10]N. S. Bakhvalov, Y. M. Zhileikin, and E. A. Zabolotskaya, "Nonlinear propagation of sound beams with a uniform amplitude distribution," Sov. Phys. Acoust. **26**, 95–100 (1980).
[11]F. A. Duck and H. C. Starritt, "The locations of peak pressures and peak intensities in finite amplitude beams from a pulsed focused transducer," Ultrasound Med. Biol. **12**, 403–409 (1986).
[12]M. A. Averkiou and M. F. Hamilton, "Nonlinear distortion of short pulses radiated by plane and focused circular pistons," J. Acoust. Soc. Am. **102**, 2539–2548 (1997).
[13]Y. N. Makov, V. J. Sánchez-Morcillo, F. Camarena, and V. Espinosa, "Nonlinear change of the on-axis pressure and intensity maxima positions and its relation with the linear focal shift effect," Ultrasonics **48**, 678–686 (2008).
[14]O. V. Bessonova, V. A. Khokhlova, M. R. Bailey, M. S. Canney, and L. A. Crum, "Focusing of high power ultrasound beams and limiting values of shock wave parameters," Acoust. Phys. **55**(4–5), 463–476 (2009).
[15]M. M. Karzova, M. V. Averiyanov, O. A. Sapozhnikov, and V. A. Khokhlova, "Mechanisms for saturation of nonlinear pulsed and periodic signals in focused acoustic beams," Acoust. Phys. **58**(1), 81–89 (2012).

[16]T. Deffieux and E. E. Konofagou, "Numerical study of practical transcranial focused ultrasound applied to blood brain barrier opening," IEEE Trans. Ultrason. Ferroelectr. Control **57**(12), 2637–2653 (2010).
[17]X. Wu and M. Sherar, "Theoretical evaluation of moderately focused spherical transducers and multi-focus acoustic lens/transducer systems for ultrasound thermal therapy," Phys. Med. Biol. **47**(9), 1603–1621 (2002).
[18]M. Fatemi and J. Greenleaf, "Ultrasound-stimulated spectrography," Science **280**, 82–85 (1998).
[19]E. E. Konofagou, J. Thierrnan, and K. Hynynen, "The use of ultrasound stimulated acoustic emission in the monitoring of modulus changes with temperature," Ultrasonics **41**, 337–345 (2003).
[20]K. Nightingale, M. Palmeri, R. Nightingale, and G. Trahey, "On the feasibility of remote palpation using acoustic radiation force," J. Acoust. Soc. Am. **110**, 625–634 (2001).
[21]C. Maleke, M. Pernot, and E. E. Konofagou, "Single-element focused ultrasound transducer method for harmonic motion imaging," Ultrason. Imaging **28**, 144–158 (2006).
[22]H. Kuttruff, *Ultrasonics Fundamentals and Application* (Elsevier, New York, 1991), p 129.
[23]Y. S. Lee and M. Hamilton, "Time-domain modeling of pulsed finite amplitude sound beams," J. Acoust. Soc. Am. **97**, 906–917 (1995).
[24]M. F. Hamilton and D. T. Blackstock, *Nonlinear Acoustics* (Academic, London, 1998), pp. 60–68.
[25]J. Naze Tjotta, S. Tjotta, and E. H. Vefring, "Effects of focusing on the nonlinear interaction between two collinear finite amplitude sound beams," J. Acoust. Soc. Am. **89**, 1017–1027 (1990).
[26]O. V. Rudenko, A. P. Sarvazyan, and S. Y. Emelianov, "Acoustic radiation force and streaming induced by focused nonlinear ultrasound in a dissipative medium," J. Acoust. Soc. Am. **99**(5), 2791–2798 (1996).
[27]O. V. Rudenko and O. A. Sapozhnikov, "Nonlinear effects limiting maximum values of acoustic fields," IEEE Ultrason. Symp. **1**, 489–491 (1992).
[28]P. V. Yuldashev and V. A. Khokhlova, "Simulation of three-dimensional nonlinear fields of ultrasound therapeutic arrays," Acoust. Phys. **57**(3), 334–343 (2011).
[29]O. Al-Bataineh, J. Jenne, and P. Huber, "Clinical and future applications of high intensity focused ultrasound in cancer," Cancer Treat. Rev. **38**(5), 346–353 (2011).
[30]A. B. Draudt and R. O. Cleveland, "Impact of nonlinear distortion on acoustic radiation force elastography," Ultrasound Med. Biol. **37**(11), 1874–1883 (2011).